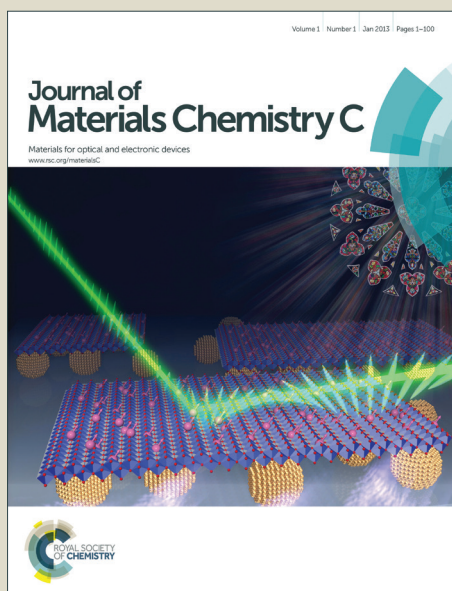


Journal of Materials Chemistry C

Accepted Manuscript



This is an *Accepted Manuscript*, which has been through the Royal Society of Chemistry peer review process and has been accepted for publication.

Accepted Manuscripts are published online shortly after acceptance, before technical editing, formatting and proof reading. Using this free service, authors can make their results available to the community, in citable form, before we publish the edited article. We will replace this *Accepted Manuscript* with the edited and formatted *Advance Article* as soon as it is available.

You can find more information about *Accepted Manuscripts* in the [Information for Authors](#).

Please note that technical editing may introduce minor changes to the text and/or graphics, which may alter content. The journal's standard [Terms & Conditions](#) and the [Ethical guidelines](#) still apply. In no event shall the Royal Society of Chemistry be held responsible for any errors or omissions in this *Accepted Manuscript* or any consequences arising from the use of any information it contains.

ARTICLE

Luminescent double helical gold(I)-thiophenolate coordination polymer obtained by hydrothermal synthesis or by thermal solid-state amorphous-to-crystalline isomerization

Cite this: DOI: 10.1039/x0xx00000x

Received 00th January 2012,
Accepted 00th January 2012

DOI: 10.1039/x0xx00000x

www.rsc.org/

Christophe Lavenn,^a Larysa Okhrimenko,^a Nathalie Guillou,^b Miguel Monge,^c Gilles Ledoux,^d Christophe Dujardin,^d Rodica Chiriac,^e Alexandra Fateeva^e and Aude Demessence^{*a}

Gold(I)-thiophenolate coordination polymer, $[\text{Au}(\text{SPh})]_n$, has been synthesized by employing hydrothermal conditions at 120 °C. This new synthesis led to isolate highly crystalline compound and to solve its structure from powder X-ray diffraction pattern. The compound forms double interpenetrated helical chains stabilized through C-H $\cdots\pi$ and aurophilic bonds. The solid is phosphorescent at room temperature and in the solid-state with a quantum yield of around 5 %. Thanks to DFT calculations, the emission is attributed to a Ligand-to-Metal-Metal Charge Transfer (LMMCT) transition with a small contribution from a Metal Centered (MC) transition. In addition to this hydrothermal reaction, it is possible to obtain this $[\text{Au}(\text{SPh})]_n$ coordination polymer by a two-step synthesis which is a thermally-induced solid-state amorphous-to crystalline isomerization. This transition has been followed by powder X-ray diffraction, scanning electron microscopy, differential scanning calorimetry and also from the appearance of phosphorescence upon heating.

Introduction

Gold thiolate is an important motif/association in material chemistry and nanotechnology.¹ Indeed the strong affinity between sulfur and gold atoms makes thiolate molecules useful to Self-Assemble Monolayers on gold surface for electronics² or as capping ligands to stabilize gold nanoparticles that find application as catalysts, sensors or biomaterials.³ More recently, atomically well-defined thiolate-protected gold nanoclusters, with $\text{Au}_n(\text{SR})_m$ formula, appear as new nanomaterials that exhibit distinct properties from gold nanoparticles.⁴ One characteristic of some of those thiolate clusters is their luminescent properties at room temperature that makes them potential materials for applications in medicine.⁵ The assumption to explain such emission is that the luminescence of gold clusters is originated from the external long $[\text{Au}(\text{I})\text{SR}]_n$ staple-like motifs surrounding the Au(0) core.⁶ Indeed gold(I) thiolate coordination polymers $[\text{Au}(\text{SR})]_n$, with mostly alkanethiolates⁷, 3-mercaptopropionic acid⁸ or arylthiolates,⁹ are known to exhibit photoluminescent properties at room temperature and are usually described as lamellar structures from their powder X-ray diffraction. The origin of the emission is ascribed to a ligand-to-metal charge transfer (LMCT) or a ligand-to-metal-metal charge transfer (LMMCT) due to the presence of aurophilic interactions.¹⁰ These Au(I)-Au(I) bonds, resulting from the strong relativistic effect of gold, are also one of the driving forces in the assembly of gold(I)-thiolates complexes.¹¹ Such weak attractive $5d^{10}$ - $5d^{10}$ interactions result into Au-Au distances ranging from 2.5 to 3.5 Å and bonding energies of 29-46 kJ/mol, comparable to hydrogen bonds. Despite

that gold(I)-thiolate complexes are (i) known for a long time because of their commercialization in diverse areas as therapeutic agents against rheumatoid arthritis¹² or as decorative inks¹³ and (ii) a key step in the Brust-Schiffin-based gold nanoparticles synthesis,¹⁴ or as precursors for nanomaterials elaboration,¹⁵ a little is known about their structures due to their insolubility. Indeed, in coordination chemistry, many structural¹⁶ and photophysical studies on gold thiolate complexes or extended networks with phosphine or nitrogen-based ligands have been reported,¹⁷ but structural details on pure $[\text{Au}(\text{SR})]_n$ coordination polymers or oligomers are limited. Among $[\text{Au}(\text{SR})]_n$ species, six oligomeric structures have been reported: $[\text{Au}(\text{SC}(\text{SiMe}_3)_3)]_4$ ¹⁸, $[\text{Au}(\text{SSi}(\text{O}^t\text{Bu})_3)]_4$ ¹⁹ and $[\text{Au}(\text{SPh}^i\text{Pr}_3)]_6$ ²⁰ that form cycles and $[\text{Au}(\text{SPh}^t\text{Bu})]_n$ ($n = 10$ and 12)²¹ and $[\text{Au}(\text{SGly})]_{11}$ ²² (SGly = a glycosylated thiolate) that are catenane rings. Among those gold(I) thiolate cyclic oligomers, $[\text{Au}(\text{SGly})]_{11}$ oligomer presents a broad weak emission at 650 nm (QY < 0.01 %) in the solid-state at room temperature. Only one structure of an extended gold thiolate coordination polymer has been reported, $\text{Na}_2\text{CsAu}_2(\text{L})(\text{LH})$, where L is the thiomalate ligand. This compound is known as the Myochrysin, a drug to treat rheumatoid arthritis.²³ The structure of this gold thiomalate polymer is described as interpenetrated double-helical chains of -Au-S-Au-S- motifs. Herein, we present a new synthetic pathway of the gold thiophenolate $[\text{Au}(\text{SPh})]_n$ coordination polymer, its structure resolution and the study of its photophysical properties. The synthesis of this $[\text{Au}(\text{SPh})]_n$ compound and its luminescent properties have already been reported by Bachman et al., but no structure resolution has been described, which prevented the

rationalization of the photophysical properties.⁹ In these previous studies, the polymeric $[\text{Au}(\text{SPh})]_n$ could be prepared at room temperature either by direct synthesis of thiophenol with HAuCl_4 in alcohol solution or by substitution reaction from isonitrile gold(I) chloride complexes $[\text{RNCAuCl}]$ to form $[\text{RNCAu}(\text{SPh})]$, followed by the loss of the isonitrile ligand. The formulation of the gold-thiophenolate polymer is the same in both reactions, but from the first one, the compound is amorphous and non-luminescent and from the second one it is crystalline and luminescent. Unluckily, due to the insolubility of the compounds, the characterizations were limited to elemental analysis, powder X-ray diffraction and light excitation/emission experiments. Being inspired by the solvothermal synthesis of coordination polymers,²⁴ we report here a new direct hydrothermal synthesis of highly crystalline and luminescent $[\text{Au}(\text{SPh})]_n$ by mixing thiophenol and HAuCl_4 . This one-step and high temperature synthetic method is the first one reported for gold(I) materials and does not require the use of gold(I) intermediates. The structure resolution from powder X-ray diffraction of $[\text{Au}(\text{SPh})]_n$, its photophysical experiments and DFT calculations are reported to correlate the structure/luminescence relationship. In addition we carried on in-depth characterizations of the thermally-induced solid-state amorphous-to-crystalline $[\text{Au}(\text{SPh})]_n$ isomerization. This study brings new insights in the understanding of the luminescence in $[\text{Au}(\text{SR})]_n$ polymers and shed light a rare example of the solid-state crystallization of a hybrid material.

Results and discussion

Hydrothermal synthesis.

The preparation of $[\text{Au}(\text{SPh})]_n$ **1a** is a hydrothermal synthesis at 150 °C for 18 hours by mixing HAuCl_4 with an excess of thiophenol (6 eq.) to get the reduction of Au(III) into Au(I) coupled with the oxidation of the thiophenol. The solid is then thoroughly washed with water and ethanol to remove the excess of thiophenol and the diphenyl disulfide molecules formed during the reaction as described in the following equation:



From powder X-ray diffraction (PXRD) (Figure 1), the phase corresponds to the already reported $[\text{Au}(\text{SPh})]_n$ coordination

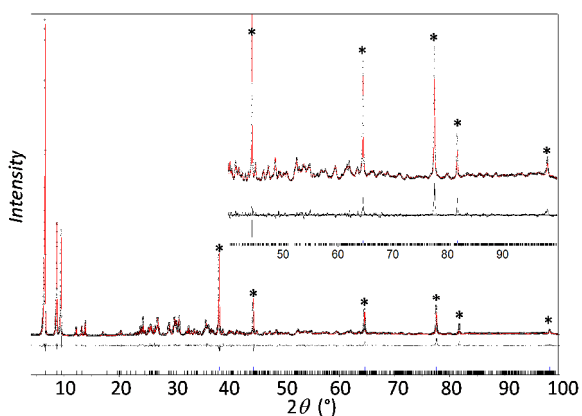


Figure 1. Final Rietveld plot of $[\text{Au}(\text{SPh})]_n$ **1a** showing observed (black circles), calculated (red line), and difference (black line) curves. A zoom at high angles is shown as inset. Stars correspond to FCC gold impurity. ($\lambda = 1.5406 \text{ \AA}$).

polymer.⁹ However as opposed to the previous two-steps reaction which consisted of the synthesis of an amorphous $[\text{Au}(\text{SPh})]_n$ polymer followed by a catalytic treatment with butyl isocyanide at room temperature, the reaction done in one-step under hydrothermal conditions, leads to better crystallinity. Nevertheless these harsher reaction conditions can also cause the formation of FCC bulk gold as impurity. After the optimization of the synthetic conditions it is possible to obtain a pure $[\text{Au}(\text{SPh})]_n$ polymer **1b** by decreasing the temperature to 120 °C for the same reaction time. These milder conditions prevent the formation of bulk gold, but also lead to a slightly less crystalline compound (Figure S1). Thus the structure resolution is performed on PXRD data of **1a**, when all other experiments are done on the pure phase of **1b**. $[\text{Au}(\text{SPh})]_n$ crystallizes in the monoclinic space group $C2/c$, with cell parameters: $a = 27.5009(7) \text{ \AA}$, $b = 4.5327(1) \text{ \AA}$, $c = 20.8032(3) \text{ \AA}$ and $\beta = 104.935(2)^\circ$ (Table 1). The structure consists in two interpenetrated helices made of infinite $-\text{Au}-\text{S}-\text{Au}-\text{S}-\text{Au}$ chains (Figure 2). This double helical geometry has already been observed for the gold thiomalate polymer. Its structure has been solved with cations coordinated to the carboxylate functions giving the formula $\text{Na}_2\text{CsAu}_2\text{L}(\text{LH})$, where L is the thiomalate ligand $[\text{O}_2\text{C}-\text{CH}_2-\text{CH}(\text{S})-\text{CO}_2]^{3-}$.²³ In the chains of $[\text{Au}(\text{SPh})]_n$, the gold atoms are coordinated to two sulfur atoms in a quasi linear fashion, S-Au-S angles are of 171.6 and 175.3 (Table 2); those angles are of 178.9 and 169.4 ° in the gold-thiomalate structure. Each thiolate function is bridging two gold cations with Au-S-Au angles: 91.4 and 102.3 °. The gold sulfur distances in $[\text{Au}(\text{SPh})]_n$ vary from 2.29 to 2.34 Å; in gold thiomalate polymer the Au-S distances are slightly shorter (2.28-2.29 Å). The gold-gold distances between the two chains are 3.33 and 3.60 Å for Au(1)-Au(2) and 3.37 and 4.03 Å for Au(1)-Au(1) and Au(2)-Au(2), respectively (Table 2 and Figure S2). Hence in this structure each gold atom from one chain interacts with three gold atoms from the second one. The two shortest Au-Au distances of 3.33 and 3.37 Å, shorter than the sum of van der Waals radii of gold atoms ($d_{vdw} \sim 3.60 \text{ \AA}$), can be considered as auriphilic interactions.¹¹ In gold thiomalate polymer structure the Au-Au interchain distance is slightly shorter of around 0.1 Å with a value of 3.23 Å. The intrachain Au-Au distances between the Au(I) bridged by thiolate ligands

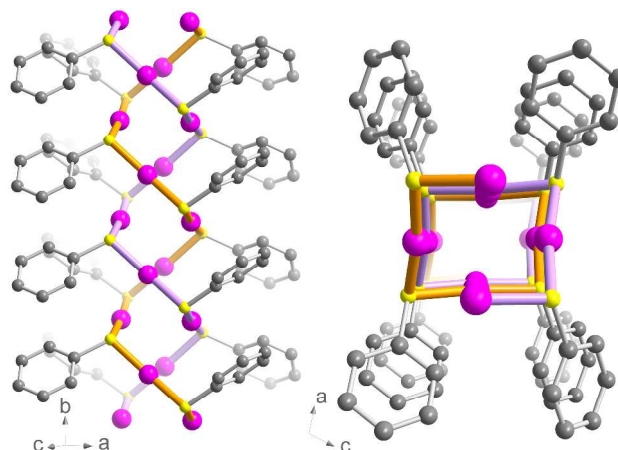


Figure 2. Structure of the $[\text{Au}(\text{SPh})]_n$ coordination polymer. On the left, view of the double helices along the b axis; both chains are represented in orange and purple colors. On the right, view of the double helices from the (ab) plan. Pink, yellow and grey spheres are gold, sulfur and carbon atoms, respectively. Hydrogen atoms have been omitted for clarity.

in $[\text{Au}(\text{SPh})]_n$ polymer are of 3.32 and 3.61 Å; those values are close to the one found in gold thiomalate compound, 3.48 Å. In addition, C-H $\cdots\pi$ interactions are observed between the parallel phenyl groups along the *b* axis.²⁵ The strongest interaction has a hydrogen to centroid of the phenyl group distance of 3.22 Å and a C-H $\cdots\pi$ angle of 107.6 ° and is present all along two phenyl chains (Figure S3). However the long C-H $\cdots\pi$ interactions of 3.76 Å observed along the two other phenyl chains and a C-H $\cdots\pi$ angle of 92.6 ° are at the limit of consideration for this kind of weak interactions. Furthermore, no interaction are observed between the packing of the double-helical chains (Figure S4). This double interdigitated helical structure remains the first one reported with a thiophenolate-based ligand and without additional cations. As a consequence, as opposed to gold thiomalate, $[\text{Au}(\text{SPh})]_n$ compound is insoluble in water and any organic solvent.

Table 1. Crystallographic data and Rietveld refinement parameters for $[\text{Au}(\text{SPh})]_n$.

Empirical formula	Au ₂ C ₁₂ H ₁₀ S ₂
M_r	612.28
Crystal system	Monoclinic
Space group	<i>C2/c</i>
<i>a</i> (Å)	27.5009(7)
<i>b</i> (Å)	4.5327(1)
<i>c</i> (Å)	20.8032(3)
β (°)	104.935(2)
<i>V</i> (Å ³)	2505.6(1)
<i>Z</i>	8
λ (Å)	1.5406
Number of reflections	1312
No. of fitted structural parameters	25
Number of soft restraints	4
R_p , R_{wp}	0.049, 0.067
R_{Bragg} , GoF	0.024, 3.79

Table 2. Distances (Å) and angles (°) selected from the structure of $[\text{Au}(\text{SPh})]_n$.[†]

Au-Au interchain distances	
Au(1)-Au(2)	3.331(3) ; 3.603(3)
Au(1)-Au(1)	3.369(3)
Au(2)-Au(2)	4.031(3)
Au-Au intrachain distances (bridged by thiolates)	
Au(1)-Au(2)	3.323(3)
Au(1)-Au(2)	3.610(3)
Au-S distances	
Au(1)-S(28)	2.289(2)

Au(1)-S(18)	2.332(2)
Au(2)-S(18)	2.313(2)
Au(2)-S(28)	2.345(2)
Au-S-Au angles	
Au(1)-S(18)-Au(2)	91.36(7)
Au(1)-S(28)-Au(2)	102.32(7)
S-Au-S angles	
S(18)-Au(2)-S(28)	171.57(9)
S(18)-Au(1)-S(28)	175.23(8)

[†]See Figure S2 for atom label assignments.

The fibrous crystallites observed by SEM are in good accordance with the 1D structure of $[\text{Au}(\text{SPh})]_n$ (Figure 3). The sticks are around 100 µm long and less than 1 µm thick. From thermo-gravimetric analysis (TGA) carried out under air, the curve (Figure S5) shows that the crystalline $[\text{Au}(\text{SPh})]_n$ compound starts to decompose at 210°C. This thermal behavior corresponds well with the values reported for the stability of gold-thiolate being between 200-300 °C.²⁶ The weight loss of the organic part of the compound **1b** is 34.9 % and the remaining metallic gold is 65.1 %. These values match well to the theoretical one expected for $[\text{Au}(\text{SPh})]_n$ compound: 35.7 and 64.3 % for the organic and gold parts, respectively. The chemical composition of **1b** is also confirmed by C, H and S elemental analyses (see experimental part). For the compound **1a** the quantity of bulk gold as impurity, obtained by TGA, elemental analysis and quantitative PXRD is around 15 wt%. FT-IR spectrum (Figure S6) presents the characteristic peaks of thiophenolate moiety, and more importantly attests of the absence of S-H stretching vibration, observed at 2550 cm⁻¹ in the free ligand, pointing out the coordination of all the thiolate groups to gold atoms.

As the structural model of $[\text{Au}(\text{SPh})]_n$ was obtained from PXRD, we studied its luminescent properties to rationalize the structure-photophysical properties relationship on gold-thiolate coordination polymer.

Crystalline gold-thiophenolate coordination polymer **1b** is luminescent and presents an intense red color when irradiated under UV lamp at room temperature (Figure 4a). On the UV-visible absorption spectrum, the absorption band is centered at 278 nm (Figure 4b). This optical transition is quite strong and is assigned to the π - π^* transition of the phenyl group of the thiophenolate.²⁷ Excitation and emission spectra have been carried out at room temperature and in the solid-state (Figure 4b). **1b** exhibits one maximum of excitation at 340 nm and a second one, less intense, at 286 nm. The position of the maximum of emission is independent of the excitation wavelength, between 250 and 400 nm, and stays centered at 684 nm (Figures 4b and S7). The position of the peaks is similar to the crystalline $[\text{Au}(\text{SPh})]_n$ material reported by Bachman et al.⁹ This emission in gold thiolate is usually assigned to a ligand to metal charge transfer (LMCT) or a ligand to metal-metal charge transfer (LMMCT) transition.²⁸

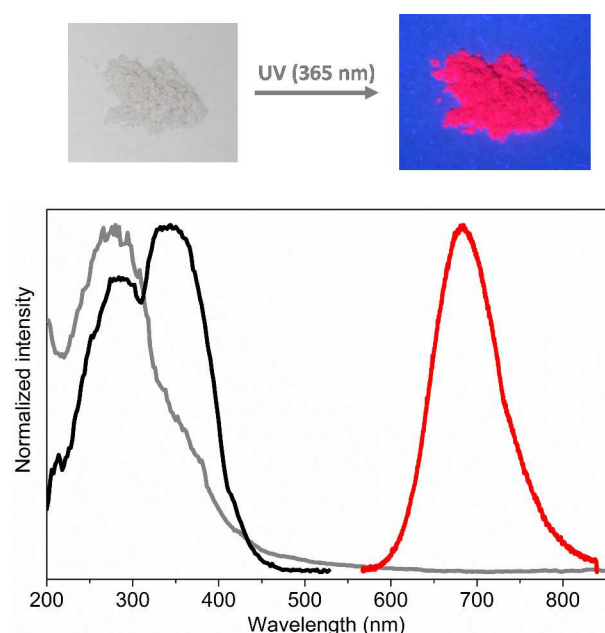


Figure 4. a. Photographs of **1b** under ambient (left) and UV (right) lights. b. Absorption (grey), excitation (black, $\lambda_{\text{em}} = \text{nm}$) and emission (red, $\lambda_{\text{ex}} = \text{nm}$) spectra of crystalline $[\text{Au}(\text{SPh})]_n$ **1b** carried out at room temperature and in solid-state.

The lifetime decay at the excited states has been measured and presents two main components of 1.178 μs (54 %) and 0.725 μs (45 %), plus a small contribution of 0.004 μs (1 %) (Figure 5). This microseconds range and the large Stokes' shift of 344 nm agree well with a phosphorescence process.²⁹ In addition, the measurement of the QY is estimated of about 5 %.

In order to rationalize the crystal structure found for $[\text{Au}(\text{SPh})]_n$ compound in the solid-state and its photoluminescent behavior, we carried out RI-DFT-D3 calculations (see Computational Details) on model system $[\text{Au}_6(\text{SPh})_8]^{2-}$ displaying a C_2 symmetry (Figures 6 and S8 and Table S1). The full optimization of this model system has been carried out by using the D3 dispersion correction to the DFT method since, as it has been shown previously, it improves the calculation of the aurophilic attraction, leading to theoretical results very close to the experimental ones.³⁰ From the optimized model system $[\text{Au}_6(\text{SPh})_8]^{2-}$ we have analyzed both the structural arrangement and the electronic structure (frontier molecular orbitals).

As it can be observed in Figure 6 the full optimization of model $[\text{Au}_6(\text{SPh})_8]^{2-}$ clearly retains the helical disposition of the trinuclear chains through unsupported aurophilic interactions. The most important optimized structural parameters agree fairly well with the experimental ones. For instance, the experimental Au-S bond distances fall in the 2.29-2.34 Å range, whereas the theoretical ones vary from 2.32 to 2.34 Å. The Au-Au distances found theoretically are also close to the experimental ones. The interchain Au(I)⋯Au(I) interaction distances vary from 3.16 to 3.39 Å (exp. 3.33-3.37 Å), whereas the intrachain S-supported Au(I)⋯Au(I) interactions appear around 3.66 Å (exp. 3.32-3.61 Å). The C-H⋯ π interactions are also observed in the optimized fragment and have a length of 2.65 and 2.97 Å (exp. 3.22 and 3.76 Å) (Figure S9). The slight differences observed between experimental and theoretical values would arise from the fact that our model system is calculated in the gas phase, where

packing effects at long distance are not taken into account, and from the terminal phenylthiolate fragment dispositions that leads to a closer interaction between the metal centers.

As it is widely known, the attraction between formally cationic Au(I) ions arises from correlation effects, which include dispersive forces, strengthened by relativistic effects.³¹ The use

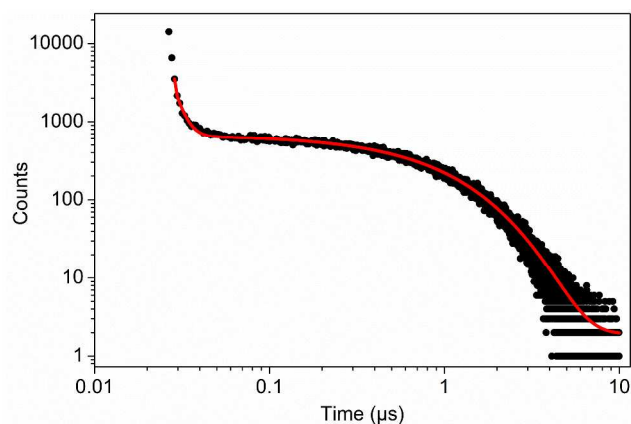


Figure 5. Luminescence lifetime of **1b** after excitation at 379 nm (black) at solid-state and room temperature. The luminescence decay was fitted to triexponential decay (red).

of this DFT-D3 approach permits to explain the experimental arrangement found for the $[\text{Au}(\text{SPh})]_n$ polymer based on the unsupported aurophilic interactions found between two infinite Au-SPh linear chains.

In a second step we have computed the highest occupied (HOMO and HOMO-1) and the lowest empty molecular orbitals (LUMO and LUMO+1) in order to check the possible origin of the emission observed experimentally for compound **1**. These orbitals are depicted in Figure 7.

As it can be observed, the HOMO and HOMO-1 orbitals are mainly located at two sulfur atoms of two of the thiolate ligands ($p\pi(\text{S})$ character), with a small contribution from the phenyl rings and the gold centers ($d\sigma^*$ character) bonded to this thiolate functional group. On the other hand, the lowest empty orbitals LUMO and LUMO+1 display a bonding molecular orbital mainly centered at the gold centers ($p\sigma$ character), with some contribution from the ligands. These theoretical observations suggest an important influence of the aurophilic interactions in the emissive behavior of polymer $[\text{Au}(\text{SPh})]_n$. As it has been mentioned above, the luminescence in gold(I)-thiolate complexes can be assigned to arise from ligand (sulfur) to metal (gold) charge transfer transitions (LMCT), in which the influence of the aurophilic interactions leads to a stabilization of the empty $p\sigma$ bonding orbital, red-shifting the emission energy.³² The character of the frontier orbitals computed for model $[\text{Au}_6(\text{SPh})_8]^{2-}$ agrees well with these assumptions. Therefore, in view of the experimental results and the shape of the highest occupied and lowest empty molecular orbitals the emissive properties of this polymeric $[\text{Au}(\text{SPh})]_n$ arrangement would arise from an admixture of a Ligand (thiolate) to Metal-Metal (gold) Charge Transfer $^3[p\pi(\text{S}) \rightarrow p\sigma(\text{Au})]$ transition with a small contribution from a Metal (gold) Centered $^3[d\sigma^*(\text{Au}) \rightarrow p\sigma(\text{Au})]$ transition. This assignment is very similar to the one previously computed for phosphine-thiolate gold(I) systems bearing aurophilic interactions.³²

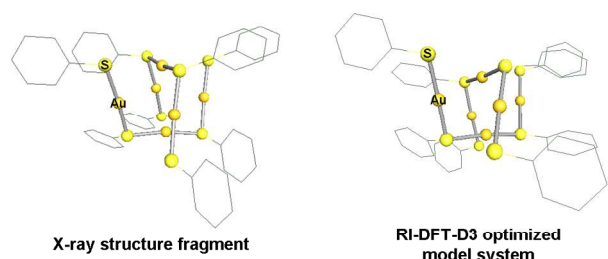


Figure 6. Comparison between the X-ray structure fragment for polymer $[\text{Au}(\text{SPh})]_n$ and model system $[\text{Au}_6(\text{SPh})_8]^{2-}$.

Even if the double helical structure has already been observed with the thiomalate ligands, the luminescence of this compound was not reported. Thus this gold thiophenolate is the first structure of a luminescent $[\text{Au}(\text{SR})]_n$ coordination polymer. This leads to understand the photophysics involved in the luminescence and reveals that the compound is phosphorescent and that the emission arise from a LMMCT transition with a small contribution from a MC transition.

Thermally-induced solid-state amorphous-to-crystalline isomerization.

To compare the hydrothermal synthesis with milder conditions, a reaction by mixing HAuCl_4 with an excess of HSPH in reflux of methanol for 20 hours has been carried out. The obtained white-off powder, compound **2**, is insoluble and the PXRD pattern presents a diagram of an amorphous compound (Figures 8 (black curves) and S10). This PXRD matches the one reported for $[\text{Au}(\text{SPh})]_n$ product by Bachman et al. and synthesized with the same reagents in methanol solution at room temperature.⁹ However, the presence of a broad peak at $2\theta = 7.7^\circ$ indicates that there is an order at small distance and a slight structuration. The distance of 1.15 nm obtained from the Bragg law may correspond to the interlamellar distance of a polymeric species or to the diameter of cyclic oligomers, like it has already been reported for $[\text{Au}(\text{SR})]_n$ oligomers ($n = 4, 6$ and $10-12$). But the insolubility of this amorphous compound supports the formation of an extended and non-structured chains of $[\text{Au}(\text{SPh})]_n$. SEM image of compound **2** on Figure 9a shows multi-faceted spheres of around 1-2 μm size. Thermal decomposition done by TG analysis gives an organic weight loss of 35.9 % and the percentage of remaining gold is 64.1 % (Figure S11). These values agree well with the organic/gold ratio of 1, and so correspond to the same formula of the crystalline **1b** compound, $[\text{Au}(\text{SPh})]_n$, meaning that they are isomers. From a structural point of view, no difference is found on the infra-red spectra (Figure S12) between **1b** and **2** $[\text{Au}(\text{SPh})]_n$ coordination polymers, confirming the same composition and close structuration. X-ray photoelectron spectroscopy (XPS) has been carried out on compound **2** to gain more information on the structure. The experimental quantification of the elements by XPS confirms also the formula of $[\text{Au}(\text{SPh})]_n$ with 1:1.04:7.86 ratios for Au:S:C atoms (expected, 1:1:6). No other elements are observed on the survey scan (Figure S13). The $4f_{7/2}$ and $4f_{5/2}$ binding energies of gold (Figure S14) are at 84.9 and 88.6 eV, respectively; the position and the sharpness of the peaks with a FWHM of 1.1 eV suggest that all gold atoms are in +I oxidation state. The white color of the compound justifies the absence of Au(0) or Au(III) and supports the formation of pure $[\text{Au}(\text{SPh})]_n$ compound. The S $2p_{3/2}$ and $2p_{1/2}$ binding energy occurring at 163.3 and 164.5 eV are typical of thiolated ligands and more importantly shows that the sulfur atoms are not oxidized (Figure S15). In addition the presence of only one peak for C1s at 284.7 eV is in good accordance with the

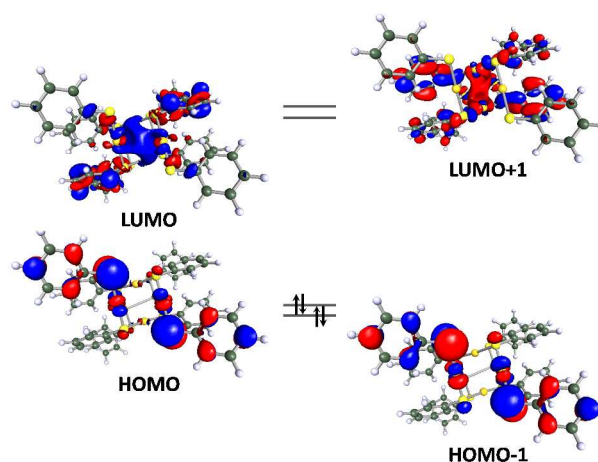


Figure 7. Frontier molecular orbitals for model system $[\text{Au}_6(\text{SPh})_8]^{2-}$.

phenyl groups (Figure S16). From photophysical point-of-view, this amorphous compound **2** exhibits a large absorption band from 230 to 440 nm (Figure S17). The appearance of a band at 350 nm, that is absent in compound **1b**, may be due to a different π -stacking of the phenyl rings. When the sample is exposed to a UV lamp and the emission spectroscopy is carried out no photophysical properties are observed at room temperature. This observation points out that even if the compounds **1b** and **2** are isomers, the differences of structure strongly impact the luminescence properties.³³

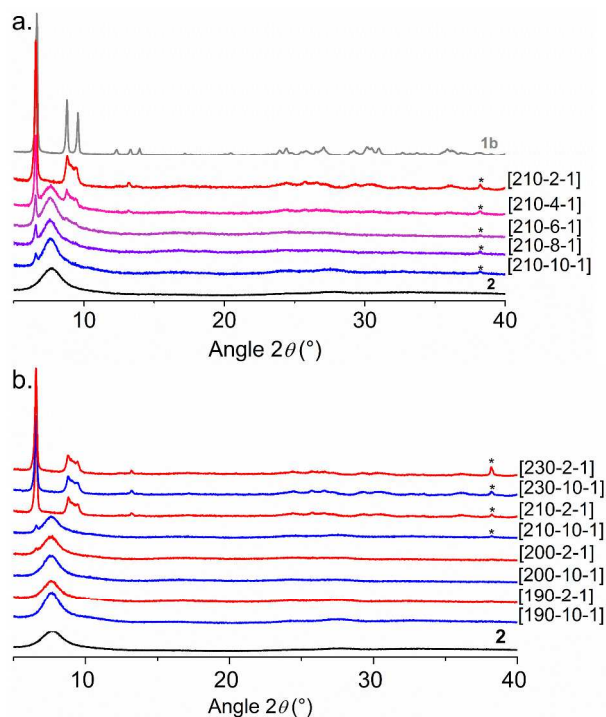


Figure 8. a. Effect of the heating rate when compound **2** is heated up to 210 $^\circ\text{C}$ for 1 s. b. Effect of the final targeted temperature 190, 200, 210 and 230 $^\circ\text{C}$ when compound **2** is heated for 1 s at 10 $^\circ\text{C}/\text{min}$ (blue) and 2 $^\circ\text{C}/\text{min}$ (red). The stars correspond to the (111) reflection of bulk gold present as

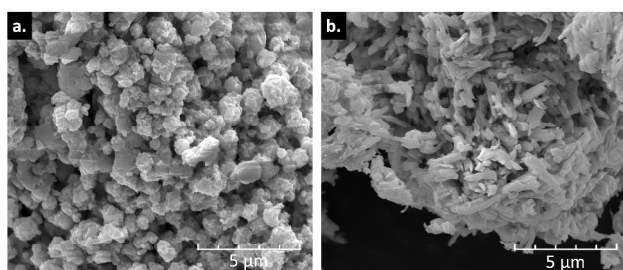


Figure 9. SEM pictures of a. compound **2** and b. compound **2** heated at 180 °C at 5 °C/min for 3 hours.

Bachman et al. also reported that it is possible to convert the amorphous and non-luminescent $[\text{Au}(\text{SPh})]_n$ into the crystalline and luminescent isomer via either a treatment with a catalytic amount of an isonitrile derivative ($< 5 \text{ mol}\%$) or by heating the compound just below its decomposition temperature.⁹ From these statements we wanted to gain more information on the thermodynamics and kinetics of this thermal amorphous-to-crystalline isomerization and carried out PXRD, DSC, SEM and emission experiments.

Thus several samples of few mg of the amorphous $[\text{Au}(\text{SPh})]_n$ compound **2**, have been heated in the solid-state. Three parameters have been studied to follow the crystallization of the compound (i) the targeted temperature (T_s , °C), (ii) the heating rate (r , °C/min) and (iii) the time at the targeted temperature (t , s), that will be noted as $[T_s-r-t]$ below. First the compound **2** has been heated at 210 °C for 1 s by applying different heating rates (10, 8, 6, 4 and 2 °C/min). On PXRD (Figure 8a), we can observe the appearance of three thin peaks between 6 and 10° and the disappearance of the broad peak of the amorphous phase at 7.7° when the heating rate is slow down from 10 to 2 °C/min. The three first main peaks at 6.6, 8.8 and 9.5°, on the PXRD of the compound heated at 210 °C at 2 °C/min, correspond to the 200, 002 and 20-2 diffraction peaks of compound **1b**, meaning the crystallization of the amorphous $[\text{Au}(\text{SPh})]_n$ into the interpenetrated double helical chains structure. Different targeted temperatures have been also applied (190, 200, 210, and 230 °C) on compound **2**, heated for 1 s and using two heating rates (2 and 10 °C/min). On Figure 8b we can see that the compound starts to crystallize from 200 °C with a heating rate of 2 °C/min and that at 230 °C there is no more amorphous phase, but bulk gold is formed. So the crystallization of the amorphous $[\text{Au}(\text{SPh})]_n$ coordination polymer in the solid state is sensitive to the targeted temperature and

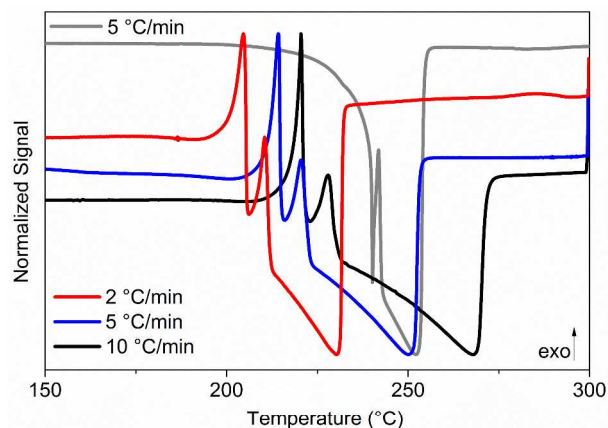


Figure 10. DSC experiments carried out under air at different heating rates (2, 5 and 10 °C/min for compound **2** (red, blue and black curves, respectively) and at 5 °C/min for compound **1b**).

the heating rate, because the transition is in competition with the decomposition of the sample. SEM pictures of the compound **2** heated at 180 °C at 5 °C/min for 3 hours and at 230 °C at 2 °C/min for 1 s (Figures 9b and S18) present the formation of needles of about 2 μm, supporting the crystallization process.

Differential scanning calorimetry (DSC) has been employed to more accurately visualize the phase transition phenomenon and evaluate the enthalpy and the activation energy of this solid-state amorphous-to-crystalline isomerization. DSC experiments have been done starting from compound **2** under air at heating rates of 2, 5 and 10 °C/min (Figure 10 and Table 3). On the three corresponding curves there are, with increasing the temperature, first two sharp exothermic peaks and then one large endothermic signal. The first strong exothermic peak, that is absent in compound **1b** and that is not associated with a weight loss, as shown on TGA experiment, is attributed to the crystallization process. This transition happens at 204.6 °C when compound **2** is heated at 2 °C/min, matching rather well the temperature of the crystalline phase formation observed on PXRD pattern (Figure 8) when it is heated at 210 °C with a 2 °C/min heating rate. PXRD patterns of compound **2** heated at 5 °C/min up to 214 °C and 216 °C, which corresponds to the maximum and the end of the first crystallization peak in the DSC experiment, exhibit the crystalline phase corresponding to the double helical structure plus the presence of bulk gold as impurities (Figure S19). The crystallization enthalpies of the exothermal transitions have been obtained by DSC experiments in J/g and then calculated to get enthalpy values in the range of $\Delta H = -2.7$ to -4.0 kJ/mol (Table 3). These values are in the order of those observed for porous coordination networks exhibiting crystalline-to-amorphous-to-crystalline phase transformations with sharp exothermic peaks denoting the crystallization process.³⁴

Table 3. Temperatures of crystallization (T_{cryst}), of the second exothermic peak (T_{exo2}) and decomposition (T_{decomp}) of compound **2** under air and upon different heating rates. In italic, data of compound **1b**.

Heating rate (°C/min)	T_{cryst} (°C)	Enthalpy (kJ/mol)	T_{exo2} (°C)	T_{decomp} (°C)
2	204.6	-2.7	210.5	230.2
5	214.2	-4.0	220.5	250.1
10	220.5	-3.5	227.8	268.0
5	-	-	<i>241.9</i>	<i>252.0</i>

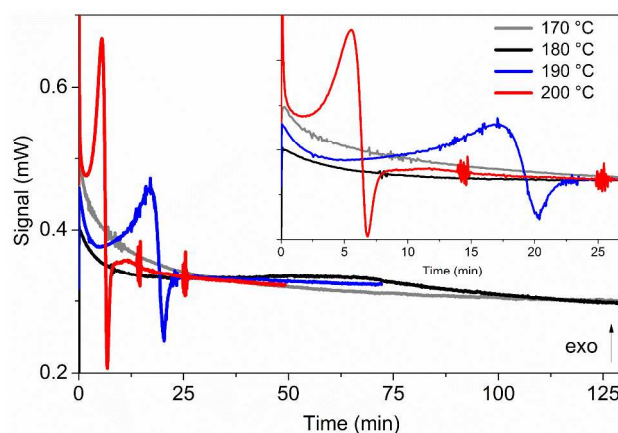


Figure 11. Isotherms followed by DSC experiments from compound **2** carried out under air at 5 °C/min at 170 (grey), 180 (black), 190 (blue) and 200 °C (red).

From DSC experiments carried out at different heating rates we can deduce the activation energy of the crystallization. An Arrhenius plot from the maximum peak position (Figure S20), gave an activation energy for the amorphous-to-crystalline phase transition of 197.3 kJ/mol.

On the three DSC curves of compound **2**, a second exothermic peak is present and shifted of 6-7 °C from the first one. This peak is also present on the crystalline **1b** solid at 241.9 °C, meaning that it corresponds to a transformation of the double helical chains. This phase transition is difficult to characterize because it is occurring in the same time as the decomposition of the crystalline structure, which is associated to the endothermic peak and the crystallization of bulk gold. Moreover, this second transition follows very closely the first transition no matter the heating rate.

The third parameter that influenced the crystallization of compound **2** is the heating time. Isotherms have been performed from the amorphous compound and have been monitored by DSC experiments (Figure 11). Heated up to 170 °C at 5 °C/min, no detectable phase transition was observed, whatever the time. From 180 °C, a large exothermic peak appears between 50 and 80 min, at 190 °C the amorphous phase starts to crystallize after 17 min of isotherm and by increasing the temperature at 200 °C the time is reduced to 5 min 30 s. This shows that it is possible to obtain the crystalline phase at lower temperature by controlling the time, but again the exothermic phase transition phenomenon is coupled with the endothermic decomposition. To clarify the nature of the solid decomposing during the isotherms, the same experiment (200 °C isotherm) was performed on the crystalline compound **1b**. For this compound no signal was detected by DSC, pointing out that the peaks are associated to the crystallization process and the decomposition of the amorphous phase only.

Samples exhibiting a thermally-induced solid-state crystallization transition become luminescent upon this phase transition. The positions of the maximum of emission peak of $[\text{Au}(\text{SPh})]_n$ obtained by heating at [210-2-1], [210-6-1] and [190-5-7200] are all centered at 692 nm (Figure S21). The small shift from the crystalline **1b** coordination polymer may be due to lower crystallization quality or presence of bulk gold. The measure of the lifetime at the excited state of $[\text{Au}(\text{SPh})]_n$ obtained by calcination of compound **2** at [210-2-1] gives two main values of 2.64 μs (76 %) and 0.603 μs (24 %), plus two components of 9 and 2 ns less than 1 % (Figure S22). Therefore when the compound is less crystalline the microsecond

time is longer and predominant.

Dynamic experiments of heating coupled with solid-state luminescence measurements have been carried out. Because the luminescence of $[\text{Au}(\text{SPh})]_n$ is quenched at high temperature ($T > 100$ °C), the emission has to be measured at 40 °C (Figure S23). By applying a heating rate of 10 °C/min on compound **2**, the emission starts to appear at 220 °C and reaches a maximum at 226 °C (Figure 12). At higher temperatures the emission decreases corresponding to the decomposition of the hybrid compound, but it is still luminescent at 255 °C. Isotherms at 200 °C with a heating rate of 10 °C/min have also been applied with the measurements of the emission at 40 °C starting from the non-luminescent compound **2** (Figure S24). The emission centered at 696 nm appears after 9 min and reaches a maximum after 27 min at 200 °C.

From these experiments, it is obvious that the appearance of the luminescence is directly associated to the crystallization of the amorphous $[\text{Au}(\text{SPh})]_n$ upon heating. The process may be the structuration of distorted and non-interacting Au-SPh chains and the formation of Au-Au interactions. Luminescence properties of $[\text{Au}(\text{SC}_2\text{H}_4\text{COOH})]_n$ polymers have also been tuned by a dynamic assembly/disassembly of the layers in function of the pH.⁸ This annealing method for the synthesis of coordination polymers remains an original way to produce new gold thiolates compounds.³⁵

Conclusions

Thanks to the use of hydrothermal conditions to synthesize $[\text{Au}(\text{SPh})]_n$, we obtain a highly crystalline product, and report the first luminescent structure of a gold(I)-thiolate coordination polymer. The structure of this compound, solved from PXRD data, is composed of two interpenetrated helical chains stabilized by aurophilic and C-H $\cdots\pi$ bonds. $[\text{Au}(\text{SPh})]_n$ is phosphorescent with a maximum of emission at 684 nm, a microsecond lifetime decay and a QY around 5 %. DFT calculations on the simulated structure show that the emission consists of a LMMCT transition due the presence of the Au(I)-Au(I) interactions. Furthermore, the thermally induced crystallization happening in the solid-state is a rare example in coordination polymers and may be used for the synthesis of new gold(I)-thiolate compounds. The results presented here significantly advance the understanding of gold thiolate coordination polymers and the different synthetic approaches offered as phase transition or phase formation (hydrothermal synthesis). The polymorphism observed for $[\text{Au}(\text{SPh})]_n$, implies different photophysical properties that can be appropriated for sensing and also shed light on the rich chemistry of thiolate gold compounds; either coordination polymers, oligomers or clusters.

Experimental

Instrumentation and methods

The structural determination of compound **1a** was carried out from X-ray powder diffraction data. Sample was introduced into a 0.5 mm capillary and spun during data collection to ensure good powder averaging. The pattern was scanned at room temperature on a Bruker D8 Advance diffractometer with a Debye-Scherrer geometry, in the 2θ range 2-100°. The D8 system is equipped with a Ge(111) monochromator producing Cu $K\alpha_1$ radiation ($\lambda = 1.540598$ Å) and a LynxEye detector. All calculations of structural investigation were performed with the TOPAS program.³⁶ The LSI-indexing method converged unambiguously to a monoclinic unit cell ($a = 27.5012(7)$, $b = 4.5326(1)$, $c = 20.8032(5)$ Å and $\beta = 104.935(2)$ ° with $M_{20} = 62$). Systematic extinctions were consistent with $C2/c$ or Cc space groups. The six unindexed lines observed on the powder

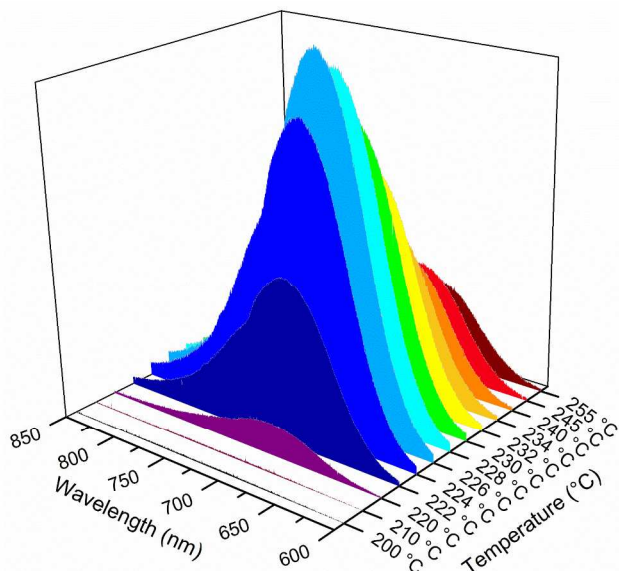


Figure 12. Emission spectra starting from the amorphous $[\text{Au}(\text{SPh})]_n$ compound and then heated at different temperature from 40 °C to 255 °C at a heating rate of 10 °C/min. All experiments are carried out in the solid-state at 40 °C with $\lambda_{\text{exc}} = 340$ nm.

pattern correspond unambiguously to the presence of gold FCC in the sample. Given the small number of lines, the presence of this impurity did not prevent us to solve the structure of compound **1a**. Indeed, at this stage the structural model of gold was taken into account and its contribution can be calculated by using the Rietveld method. The quantitative amount of bulk gold was estimated at about 14 wt%. Simultaneously, a list of 887 reflections was extracted in the angular range $4\text{--}85^\circ$ (2θ) with the Pawley method and used to initialize the structural investigation of $[\text{Au}(\text{SPh})]_n$ by means of the charge flipping method. That allowed location of two independent gold atoms on general positions in the centrosymmetric space group. The direct space strategy was then used to complete the structural model and two independent organic moieties have been added to the fixed gold atomic coordinates and treated as rigid bodies in the simulated annealing process. The use of 2 objects restricts the number of parameters to 13 (1 scale factor, 3 parameters for the orientation of each object and 3 others for the translation of the organic moiety on general position). Calculations converged to $R_B = 0.053$ and $R_{wp} = 0.143$. This structural model was used as the starting model in the Rietveld refinement. At its final stage (table 1 and Figure 1), it involved the following structural parameters: 6 atomic coordinates, 6 translation and 6 rotation parameters for organic moieties as well as 4 distances in the rigid bodies, 2 thermal factors and 1 scale factor. CCDC-1042161 contains the supplementary crystallographic data for $[\text{Au}(\text{SPh})]_n$ compound. These data can be obtained free of charge from The Cambridge Crystallographic Data Centre via www.ccdc.cam.ac.uk/data_request/cif.

Routine X-ray diffraction (XRD) was carried out on a Bruker D8 Advance A25 diffractometer using Cu K α radiation equipped with a 1-dimensional position-sensitive detector (Bruker LynxEye). XR scattering was recorded between 4° and 90° (2θ) with 0.02° steps and 0.5 s per step (28 min for the scan). Divergence slit was fixed to 0.2° and the detector aperture to 189 channels (2.9°).

Thermo-gravimetric analysis (TGA) and differential thermal analysis (DTA) were performed with a TGA/DSC 1 STARe System from Mettler Toledo. Around 2 mg of sample was heated at a rate of $10^\circ\text{C}\cdot\text{min}^{-1}$, in a $70\ \mu\text{L}$ alumina crucible, under air or nitrogen atmosphere ($20\ \text{mL}\cdot\text{min}^{-1}$). Shining droplets of bulk gold were observed at the end of experiment.

The infrared spectra were obtained from a Bruker Vector 22 FT-IR spectrometer with KBr pellets at room temperature and registered from $4000\ \text{cm}^{-1}$ to $400\ \text{cm}^{-1}$.

Sulphur percentage is determined by full combustion at $1320\text{--}1360^\circ\text{C}$ under O_2 stream and analysis of SO_2 and is titrated in a coulometric-acidimetric cell. Carbon and hydrogen percentage is determined by full combustion at $1030\text{--}1070^\circ\text{C}$ under O_2 stream and transformed into CO_2 and H_2O and is titrated on a coulometric detector. Analysis precision is 0.3% absolute for carbon, sulphur and hydrogen.

Images from Figure 3 have been recorded with a scanning electron microscope JEOL LV 5800 and pictures from Figures 9 and S18 were obtained with FEI Quanta 250 FEG scanning electron microscope, samples were mounted on stainless pads and sputtered with Au/Pd alloy to prevent charging during observation.

Absorption spectra were recorded on a Perkin Elmer Lambda 35 UV/VIS spectrometer equipped with an integration sphere for solid-state experiments. Measurements have been registered from 900 to 200 nm with a 2 nm slit at $1920\ \text{nm}/\text{min}$ and an interval of 2 nm.

The photoluminescence was performed on a homemade apparatus. The sample was illuminated by a EQ99X laser driven light source filtered by a Jobin Yvon Gemini 180 monochromator. The exit slit from the monochromator was then reimaged on the sample by two 100m focal length, 2 inch diameter MgF_2 lenses. The whole

apparatus has been calibrated by means of a Newport 918D Low power calibrated photodiode sensor over the range 190–1000 nm. The resolution of the system being 4 nm. The emitted light from the sample is collected by an optical fiber connected to a Jobin-Yvon TRIAX320 monochromator equipped with a cooled CCD detector. At the entrance of the monochromator different long pass filter can be chosen in order to eliminate the excitation light. The resolution of the detection system is 2 nm. To perform luminescence lifetime measurements, the sample was excited by a pulsed laser diode from Hamamatsu, with a central wavelength at 379 nm, a peak power of 742 mW and pulses of 51 ps. The repetition rate used for the experiment here was 50 kHz. The luminescence from the sample was collected with a lens, filtered by a high pass filter (FELH600 from Thorlabs) and fed to a PMA182 photomultiplier connected to a PicoHarp-300 TCSPC module both from picoquant. The overall timing resolution is in the order of 200 ps. Luminescence quantum yield was estimated by the same procedure as described previously and is mentioned in the ESI and Figure S25.³⁷

All calculations were carried out using TURBOMOLE version 6.4.³⁸ The polymer $[\text{Au}(\text{SPh})]_n$ was studied through the full optimization of the anionic hexanuclear model system $[\text{Au}_6(\text{SPh})_8]^{2-}$ (102 atoms) representing the arrangement observed experimentally through the disposition of two trinuclear $[\text{Au}_3(\text{SPh})_4]^-$ units in a helical fashion and with terminal SPh^- ligands in order to keep the linear Au(I) coordination environment. The hybrid PBE functional³⁹ was used together with the D3 dispersion correction previously described by Grimme.⁴⁰ In order to keep the computational cost feasible we have taken advantage of the Resolution of the Identity (RI) approximation Density Functional Theory, which improves the computational efficiency of large-scale calculations.⁴¹ Therefore, this computational approach was abbreviated as RI-DFT-D3. All atoms were described by using a triple-zeta-valence quality basis sets with polarization function (def2-TZVP).⁴² In the case of gold the core electrons were described using a 60-electron relativistic effective core potential.⁴³

Differential scanning calorimetry measurements were carried out with a DSC 820 Mettler Toledo. The following experimental conditions have been considered: sample mass of about 5 mg, aluminium crucible of $40\ \mu\text{L}$ with a pinhole, heating rate of 2, 5 and $10^\circ\text{C}\cdot\text{min}^{-1}$, temperature range of $25\text{--}300^\circ\text{C}$ and air atmosphere ($30\ \text{mL}\cdot\text{min}^{-1}$). The DSC device was calibrated over the range $25\text{--}400^\circ\text{C}$, and the melting points and enthalpies of standards (*i.e.* indium and zinc) were used for the calibration in terms of heat flow, temperature and tau lag. The samples were analysed three times to ensure result reproducibility. To exploit the obtained thermograms, the Mettler Toledo STAR 10.1 software was used.

X-ray photoelectron spectroscopy (XPS) experiment was carried out on a KRATOS Axis Ultra DLD spectrometer using monochromated Al K α source ($h\nu = 1486.6\ \text{eV}$, 150 W), a pass energy of 20 eV, a hybrid lens mode and an indium sample holder in ultra-high vacuum ($P < 10^{-9}$ mbar). The analyzed surface area was $300\ \mu\text{m} \times 700\ \mu\text{m}$. Charge neutralization was required for all samples. Scan survey was done at an energy of 160 eV and the elements Au 4f, S 2p and C 1s at 20 eV. The peaks (Au 4f, S 2p) were referenced to the aromatic carbon atoms components of the C 1s band at 284.7 eV. Shirley background subtraction and peak decomposition using Gaussian–Lorentzian products were performed with the Vision 2.2.6 Kratos processing program.

Chemicals and synthesis

Tetrachloroauric acid trihydrate ($\text{HAuCl}_4 \cdot 3\text{H}_2\text{O}$, $\geq 49\%$ Au basis), thiophenol ($\geq 99\%$) and methanol (Chromasolv®) were purchased from Sigma-Aldrich Company and were used without

further purification. All reactions were carried out in atmospheric conditions.

Synthesis of compound 1a. HAuCl₄·3H₂O (130 mg, 0.33 mmol, 1 eq) was dissolved in 10 ml of water and added with thiophenol (202 μl, 1.98 mmol, 6 eq) in a 23 mL Teflon-lined autoclave. The mixture was then sealed and heated at 150 °C for 18 h. The obtained pale pink powder was filtered and washed thoroughly with water and ethanol. Elemental analysis for Au_{1.3}C₆H₅S exp. (calc.) wt%: C 19.77 (19.73), H 1.31 (1.38), S 8.98 (8.78). The excess of gold (16.2 wt%) is due to the presence of bulk gold as impurities. TGA for [Au(SPh)]_n exp. (calc.) wt%: organic part 30.2 (35.7), residual gold 69.8 (64.3), the deduced excess of bulk gold as impurity is 15.3 wt%.

Synthesis of compound 1b. HAuCl₄·3H₂O (130 mg, 0.33 mmol, 1 eq) was dissolved in 10 ml of water and added with thiophenol (202 μl, 1.98 mmol, 6 eq) in a 23 mL Teflon-lined autoclave. The mixture was then sealed and heated at 120 °C for 18 h. The obtained white powder was filtered and washed thoroughly with water and ethanol. The amount of [Au(SPh)]_n compound was 98 mg (yield of 97 % based on gold). Elemental analysis: AuC₆H₅S exp. (calc.) wt%: C 23.75 (23.54), H 1.60 (1.65), S 11.05 (10.47). TGA for [Au(SPh)]_n exp. (calc.) wt%: organic part 34.9 (35.66), residual gold 65.1 (64.34).

Synthesis of compound 2. HAuCl₄·3H₂O (200 mg, 1 eq, 528 μmol Au basis) was dissolved in 70 mL of methanol and added in a 250 mL round-bottom flask equipped with a condenser. Thiophenol (320 μl, 6 eq, 3.13 mmol) was introduced to the solution. The mixture was then heated at reflux and left under stirring for 20 hours. The white-off product was recovered by centrifugation (4,000 rpm, 10 min) and washed with methanol and collected via centrifugation again. The last step was repeated three times in order to completely remove the salts and the disulfides formed. The amount of [Au(SPh)]_n compound was 157 mg (yield of 95 % based on gold).

Acknowledgements

CL thanks the French ministry for his PhD grant. Authors gratefully acknowledge N. Cristin and P. Mascunan for elemental analysis, L. Cardenas for XPS experiments and the CTμ (Centre technologique des Microstructures) of the University of Lyon 1 for providing scanning electron microscopy. Institut de Chimie de Lyon is thanked for its financial support. M. M. thanks the DGI Project MINECO/FEDER (CTQ2013-48635-C2-2-P) for financial support.

Notes and references

^a Institut de Recherches sur la Catalyse et l' Environnement de Lyon (IRCELYON), UMR CNRS 5256, Université Claude Bernard Lyon 1, Villeurbanne, France. E-mail: aude.demessence@ircelyon.univ-lyon1.fr.

^b Institut Lavoisier de Versailles (ILV), UMR CNRS 8180, Université de Versailles Saint-Quentin-en-Yvelines, Versailles, France.

^c Departamento de Química, Universidad de La Rioja. Centro de Investigación en Síntesis Química (CISQ). Complejo Científico-Tecnológico, Logroño, Spain.

^d Institut Lumière Matière (ILM), UMR CNRS 5306, Université Claude Bernard Lyon 1, Villeurbanne, France.

^e Laboratoire des Multimatériaux et Interfaces (LMI), UMR CNRS 5615, Université Claude Bernard Lyon 1, Villeurbanne, France.

Electronic Supplementary Information (ESI) available: details of characterizations of the coordination polymers (PXRD, schemes of the structure, TGA, FT-IR, absorption, excitation and emission spectroscopies, [Au₆(SPh)₈]²⁻ theoretical model, XPS, SEM and QY); see DOI: 10.1039/b000000x/

- H. Häkkinen, *Nature Chem.*, 2012, **4**, 443.
- J. C. Love; L. A. Estroff; J. K. Kriebel; R. G. Nuzzo; G. M. Whitesides, *Chem. Rev.*, 2005, **105**, 1103.

- (a) M. C. Daniel; D. Astruc, *Chem. Rev.*, 2004, **104**, 293; (b) C. Xue; Y. Xue; L. Dai; A. Urbas; Q. Li, *Adv. Optical Mater.*, 2013, **1**, 581; (c) M. Haruta, *Angew. Chem. Int. Ed.*, 2014, **53**, 52.
- (a) P. D. Jadzinsky; G. Calero; C. J. Ackerson; D. A. Bushnell; R. D. Kornberg, *Science*, 2007, **318**, 430; (b) H. F. Qian; M. Z. Zhu; Z. K. Wu; R. C. Jin, *Acc. Chem. Res.*, 2012, **45**, 1470; (c) T. Tsukuda, *Bull. Chem. Soc. Jpn*, 2012, **85**, 151.
- (a) J. Zheng; C. Zhou; M. Yu; J. Liu, *Nanoscale*, 2012, **4**, 4073; (b) Z. Luo; K. Zheng; J. Xie, *Chem. Commun.*, 2014, **50**, 5143.
- (a) Z. Luo; X. Yuan; Y. Yu; Q. Zhang; D. T. Leong; J. Y. Lee; J. Xie, *J. Am. Chem. Soc.*, 2012, **134**, 16662; (b) A. Das; T. Li; G. Li; K. Nobusada; C. Zeng; N. L. Rosi; R. Jin, *Nanoscale*, 2014, **6**, 6458; (c) Y. Yu; Z. Luo; D. M. Chevrier; D. T. Leong; P. Zhang; D. Jiang; J. Xie, *J. Am. Chem. Soc.*, 2014, **136**, 1246.
- (a) S.-H. Cha; J.-U. Kim; K.-H. Kim; J.-C. Lee, *Chem. Mater.*, 2007, **19**, 6297; (b) S.-H. Cha; K.-H. Kim; W.-K. Lee; J.-C. Lee, *J. Ind. Eng. Chem.*, 2010, **16**, 816.
- H. Nie; M. Li; Y. Hao; X. Wang; S. X.-A. Zhang, *Chem. Sci.*, 2013, **4**, 1852.
- (a) R. E. Bachman; S. A. Bodolosky-Bettis; S. C. Glennon; S. A. Sirchio, *J. Am. Chem. Soc.*, 2000, **122**, 7146; (b) R. E. Bachman; S. A. Bodolosky-Bettis, *Z. Naturforsch.*, 2009, **64b**, 1491.
- V. W.-W. Yam; K. K.-W. Lo, *Chem. Soc. Rev.*, 1999, **28**, 323.
- (a) P. Pykkö, *Chem. Rev.*, 1997, **97**, 597; (b) S. Sculfort; P. Braunstein, *Chem. Soc. Rev.*, 2011, **40**, 2741; (c) H. Schmidbauer; A. Schier, *Chem. Soc. Rev.*, 2012, **41**, 370.
- C. F. Shaw III, *Chem. Rev.*, 1999, **99**, 2589.
- P. T. Bishop, *Gold Bull.*, 2002, **35**, 89.
- C. Yu; L. Zhu; R. Zhang; X. Wang; C. Guo; P. Sun; G. Xue, *J. Phys. Chem. C*, 2014, **118**, 10434.
- H. Nie; M. Li; Y. Hao; X. Wang; S. Gao; B. Yang; M. Gu; L. Sun; S. X.-A. Zhang, *J. Colloid Interface Sci.*, 2014, **434**, 104.
- R. J. Puddephatt, *Coord. Chem. Rev.*, 2001, **216-217**, 313.
- (a) J. M. Forward; D. Bohmann; J. P. Fackler, Jr.; S. R. J., *Inorg. Chem.*, 1995, **34**, 6330; (b) W. B. Jones; J. Yuan; R. Narayanaswamy; M. A. Young; R. C. Elder; A. E. Bruce; M. R. M. Bruce, *Inorg. Chem.*, 1995, **34**, 1996.
- P. J. Bonasia; D. E. Gindelberger; J. Arnold, *Inorg. Chem.*, 1993, **32**, 5126.
- W. Wojnowski; B. Becker; J. Sassmannshausen; E.-M. Peters; K. Peters; H. G. Von Schnering, *Z. Anorg. Allg. Chem.*, 1994, **620**, 1417.
- I. Schröter; J. Strähle, *Chem. Ber.*, 1991, **124**, 2161.
- M. R. Wiseman; P. A. Marsh; P. T. Bishop; B. J. Brisdon; M. F. Mahon, *J. Am. Chem. Soc.*, 2000, **122**, 12598.
- S. S. Chui; R. Chen; C. Che, *Angew. Chem. Int. Edit.*, 2006, **45**, 1621.
- R. Bau, *J. Am. Chem. Soc.*, 1998, **120**, 9380.
- (a) A. Demessence; G. Rogez; R. Welter; P. Rabu, *Inorg. Chem.*, 2007, **46**, 3423; (b) T. Ahnfeldt; N. Guillou; D. Gunzelmann; I. Margiolaki; T. Loiseau; G. Férey; J. Senker; N. Stock, *Angew. Chem. Int. Ed.*, 2009, **48**, 5163.
- M. Nishio, *Phys. Chem. Chem. Phys.*, 2011, **13**, 13873.
- S.-H. Cha; K.-H. Kim; J.-U. Kim; W.-K. Lee; J.-C. Lee, *J. Phys. Chem. C*, 2008, **112**, 13862.
- J. S. Lim; H. Choi; I. S. Lim; S. B. Park; Y. S. Lee; S. K. Kim, *J. Phys. Chem. A*, 2009, **113**, 10410.
- E. R. T. Tiekink; J.-G. Kang, *Coord. Chem. Rev.*, 2009, **253**, 1627.
- V. Balzani; P. Ceroni; A. Juris, *Photochemistry and Photophysics: Concepts, Research, Applications*. Wiley-VCH: 2014.
- M. Andrejic; R. A. Mata, *Phys. Chem. Chem. Phys.*, 2013, **15**, 18115.
- P. Pykkö; Y. Zhao, *Angew. Chem. Int. Ed.*, 1991, **30**, 604.
- E. J. Fernández; A. Laguna; J. M. López-de-Luzuriaga; M. Monge; E. Sánchez-Forcada, *Dalton Trans.*, 2011, **40**, 3287 and references therein.
- S. Varughese, *J. Mater. Chem. C*, 2014, **2**, 3499.
- J. Marti-Rujas; N. Islam; D. Hashizume; F. Izumi; M. Fujita; M. Kawano, *J. Amer. Chem. Soc.*, 2011, **133**, 5853.
- J. Marti-Rujas; M. Kawano, *Acc. Chem. Res.*, 2013, **46**, 493.
- Topas V4.2: General Profile and Structure Analysis Software for Powder Diffraction Data, Bruker AXS Ltd, 2008.

37. S. Mishra; E. Jeanneau; G. Ledoux; S. Daniele, *Inorg. Chem.*, 2014, **53**, 11721.
38. R. Ahlrichs; M. Bär; M. Häser; H. Horn; C. Kölmel, *Chem. Phys. Lett.*, 1989, **162**, 165.
39. J. P. Perdew; K. Burke; M. Ernzerhof, *Phys. Rev. Lett.*, 1996, **77**, 3865.
40. S. Grimme; J. Antony; S. Ehrlich; H. Krieg, *J. Chem. Phys.*, 2010, **132**, 154104.
41. M. Feyereisen; G. Fitzgerald; A. Komornicki, *Chem. Phys. Lett.*, 1993, **208**, 359.
42. F. Weigend; R. Ahlrichs, *Phys. Chem. Chem. Phys.*, 2005, **7**, 3297.
43. D. Andrae; U. Häussermann; M. Dolg; H. Stoll; H. Preuss, *Theor. Chem. Acc.*, 1990, **77**, 123.

Graphical Abstract:

First structure of a luminescent gold thiolate coordination polymer, $[\text{Au}(\text{SPh})]_n$, synthesized in hydrothermal conditions and that can be prepared from a rare thermally-induced solid-state amorphous-to-crystalline transition.

